

Modelling the signal delivered by a population of first-order neurons in a moth olfactory system

Article (Accepted Version)

Grémiaux, Alexandre, Nowotny, Thomas, Martinez, Dominique, Lucas, Philippe and Rospars, Jean-Pierre (2012) Modelling the signal delivered by a population of first-order neurons in a moth olfactory system. *Brain Research*, 1434. pp. 123-135. ISSN 0006-8993

This version is available from Sussex Research Online: <http://sro.sussex.ac.uk/38437/>

This document is made available in accordance with publisher policies and may differ from the published version or from the version of record. If you wish to cite this item you are advised to consult the publisher's version. Please see the URL above for details on accessing the published version.

Copyright and reuse:

Sussex Research Online is a digital repository of the research output of the University.

Copyright and all moral rights to the version of the paper presented here belong to the individual author(s) and/or other copyright owners. To the extent reasonable and practicable, the material made available in SRO has been checked for eligibility before being made available.

Copies of full text items generally can be reproduced, displayed or performed and given to third parties in any format or medium for personal research or study, educational, or not-for-profit purposes without prior permission or charge, provided that the authors, title and full bibliographic details are credited, a hyperlink and/or URL is given for the original metadata page and the content is not changed in any way.

NOTICE: this is the author's version of a work that was accepted for publication in Brain Research. Changes resulting from the publishing process, such as peer review, editing, corrections, structural formatting, and other quality control mechanisms may not be reflected in this document. Changes may have been made to this work since it was submitted for publication. A definitive version was subsequently published in Brain Research 1434:123-35, Jan 24, 2012. doi: 10.1016/j.brainres.2011.09.035

MODELLING THE SIGNAL DELIVERED BY A POPULATION OF FIRST-ORDER NEURONS IN A MOTH OLFACTORY SYSTEM

Alexandre Grémiaux^a, Thomas Nowotny^b, Dominique Martinez^{a,c},
Philippe Lucas^a and Jean-Pierre Rospars^a

^a UMR 1272 Physiologie de l'insecte, INRA, Versailles, France

^b Informatics, University of Sussex, Brighton, United Kingdom

^c CORTEX Team, LORIA, Vandœuvre-lès-Nancy, France

Corresponding author:

Dr. Jean-Pierre Rospars, UMR 1272 Physiologie de l'insecte, INRA, route de Saint-Cyr,
78026 Versailles Cedex, France, Phone: +33-1-30 83 33 55, Fax: +33-1-30 83 31 19,
E-mail: jean-pierre.rospar@versailles.inra.fr

E-mail addresses:

Alexandre Gremiaux [alexandre.gremiaux@versailles.inra.fr]

Thomas Nowotny [T.Nowotny@sussex.ac.uk]

Dominique Martinez [Dominique.Martinez@loria.fr]

Philippe Lucas [philippe.lucas@versailles.inra.fr]

Jean-Pierre Rospars [jean-pierre.rospar@versailles.inra.fr]

Highlights

- > Odour intensity coding in a whole population of moth receptor neurons was modelled.
- > Frequency (spikes per second) and latency of the first spike were analyzed
- > The model accounts for the statistical distributions of frequencies and latencies.
- > The same dose-frequency relation applies at the single cell and population levels.
- > Predictions based on a biophysical model of frog olfactory neurons are confirmed.

Abstract. A statistical model of the population of first-order olfactory receptor neurons (ORNs) is proposed and analysed. It describes the relationship between stimulus intensity (odour concentration) and coding variables such as rate and latency of the population of several thousand sex-pheromone sensitive ORNs in male moths. Although these neurons likely express the same olfactory receptor, they exhibit, at any concentration, a relatively large heterogeneity of responses in both peak firing frequency and latency of the first action potential fired after stimulus onset. The stochastic model is defined by a multivariate distribution of six model parameters that describe the dependence of the peak firing rate and the latency on the stimulus dose. These six parameters and their mutual linear correlations were estimated from experiments in single ORNs and included in the multidimensional model distribution. The model is utilized to reconstruct the peak firing rate and latency of the message sent to the brain by the whole ORN population at different stimulus intensities and to establish their main qualitative and quantitative properties. Finally, these properties are shown to be in agreement with those found previously in a vertebrate ORN population.

Keywords: olfactory receptor neuron; neural population; rate coding; temporal coding; insect; sexual pheromone.

Accepted 17 September 2011

Available on line 24 September 2011

Doi: 10.1016/j.brainres.2011.09.035

1. INTRODUCTION

Insects constitute well-suited model organisms to unravel olfactory codes. They share with vertebrates a common design of their olfactory system with similar molecular and cellular organizations and conserved mechanisms for olfactory coding (Davis, 2004; Hildebrand and Shepherd, 1997; Jacquin-Joly and Lucas, 2005; Kay and Stopfer, 2006; Strausfeld and Hildebrand, 1999). Odorant compounds bind to receptor proteins on the ciliary surface of olfactory receptor neurons (ORNs) located in a large number of antennal sensilla. The ORN axons project to the antennal lobe in the brain where they make synaptic contacts with cerebral neurons within discrete, spherical neuropils called glomeruli. In *Drosophila* all ORNs projecting to a given glomerulus express the same receptor protein and each ORN projects only to one or in exceptional cases a few glomeruli (Vosshall et al., 2000), which explains that glomeruli in insects are individually identifiable (Rospars, 1988).

This general organization is common to the generalist subsystem, which is sensitive to many odorants (originating from food, predators, etc.), and to the specialist subsystem, which is sensitive to pheromones. In moths, for example, females release specific odour blends – sex pheromones – to signal their presence to males. Males in turn use their pheromone subsystem to locate them. The population of ORNs in the pheromone subsystem (~10,000) converges onto a smaller number of central neurons (~100, Homberg et al., 1988). In particular, the ORNs sensitive to the major component of the pheromone blend, the most common in the moth antenna, project to a single glomerulus of the MGC, the cumulus (Hansson et al., 1992). The pheromone subsystem of male moths shares all major properties of the generalist olfactory system of both insects and vertebrates, yet in a form well amenable to investigations with well-characterized ligands, highly specific receptors, and a large number of specialized, identical and identifiable ORNs. These features account for the traditional importance of the moth pheromone system in olfactory research (reviewed by de Bruyne and Baker, 2008; Jacquin-Joly and Lucas, 2005; Kaissling 2004).

The aim of the present work was to develop a model of the population of ORNs responding to the main component of the pheromone blend. Modelling the ORN population has received relatively little attention (Sandström et al., 2009), whereas the antennal lobe (AL) network has been frequently studied (see e.g. Bazhenov et al. 2001; Cleland and Linster 2005; Christensen et al. 2001; Martinez 2005; Rospars and Fort 1994; Simoes de Souza and Antunes 2007; Ito et al. 2009; Zavada et al 2011). However the two subjects are linked because modelling the activity of the AL neural network requires a detailed knowledge of the input it receives from the ORN population (Ito et al. 2009; Raman et al. 2010). There are two challenges to modelling this input: First, it has to be reconstructed from ORN recordings in many individuals because no electrophysiological technique permits its direct observation in a single animal. Second, any model has to take into account the heterogeneity of ORN responses, even for ORNs expressing the same receptor, as shown in vertebrates (Grosmaître et al., 2006) and in insects (Jarriault et al., 2010). It follows that the cellular level of single neurons must be linked to the population level and stochastic aspects must be taken into account. These two needs make modelling a promising approach to unravel the properties of the overall olfactory message.

The present modelling work was based on statistical data obtained from experimental recordings of first-order neurons responding to the main pheromone component in the moth *Agrotis ipsilon*. These data (Grémiaux et al., in preparation) were utilized to constrain and validate the model of the ORN population presented here. The resulting model differs from our previous work on population coding (Sandström et al., 2009) in two aspects: the biological substrate, which previously was the frog generalist olfactory system, and the modelling approach, which previously was based on a biophysical ORN model and did not

take latency into account. Although the absolute latency cannot be known by the brain, it has been shown that the first responding neurons can be a reliable cue to generate an internal reference for stimulus onset (Chase and Young, 2007) and that the relative latencies between neurons in a population can code for both odour identity and concentration (Krofczik et al., 2009; Junek et al., 2010). Here, the model is essentially phenomenological and does not consider the molecular and cellular mechanisms that give rise to the observed trains of action potentials. The comparison of the overall properties of the peripheral olfactory rate code derived from these almost independent approaches, and the extension to the latency code, were two motivations for the present work.

2. MODEL

2.1. Experimental data

All experimental data (nature of dose-response functions, their parameter values and statistical distributions) were reported elsewhere (Grémiaux et al., in preparation). Only information needed to understand the stochastic model described in section 2.3 are given here. The experimental data come from single-sensillum electrophysiological recordings of ORNs sensitive to the main pheromone compound (*cis*-7-dodecenyl acetate, Z7-12:OAc) of the moth *Agrotis ipsilon*, using the tip recording technique (Jarriault et al. 2010; Grémiaux et al., in preparation). Briefly, the stimulus was delivered as square pulses of 200 ms duration at different doses. The dose C was expressed as the decimal logarithm of the mass m of Z7-12:OAc (in ng) deposited on a filter paper in the stimulating device, $C = \log m$. (Throughout the paper we denote the decimal logarithm as ‘log’ and the natural logarithm as ‘ln’). The experimental relative variability on C at the vicinity of the sensillum was estimated to ~20%, so $\sigma_C = 0.2C$. This uncertainty is relatively small with respect to the interval between the successive doses tested ($\delta C = 1$) and their wide overall range.

Each ORN was tested at six doses from -1 to 4 log ng yielding recordings as shown in **Fig. 1**. An ORN was considered as responding if a peak firing rate at least 1.25-fold higher than its mean spontaneous activity was fired after stimulus onset. When a response was detected, the instantaneous frequency f of each spike was calculated as the inverse of the corresponding inter-spike interval. The frequency F of the peak was determined as the mean of the first 3 instantaneous frequencies in the subset of the 20% largest f 's. Latency L was determined as the time elapsed from odorant delivery to the first spike in the response. If no response was detected, F was considered as zero and L was not defined.

2.2. Model of a single ORN

All aspects of the spike train fired by an ORN in response to a short constant stimulation of pheromone depend on the applied dose C (**Fig. 1**), especially variables F and L defined above. The dose-response functions $F(C)$ and $L(C)$ of each ORN were characterized by a set of 6 response parameters: F_M , $C_{1/2}$, n , L_a , L_m and λ as done previously for frog recordings (Rosparis et al., 2003).

The frequency F (AP.s⁻¹) at which an ORN fires action potentials increases with the pheromone dose C from zero to a horizontal asymptote F_M . This sigmoid function $F(C)$ is well described by a Hill function with 3 parameters F_M , $C_{1/2}$ and n (**Fig. 2a**):

$$F(C) = \frac{F_M}{1 + \exp(-\ln(10)n(C - C_{1/2}))}, \quad (1)$$

where F_M is the asymptotic maximum frequency, $C_{1/2}$ is the dose at half-maximum frequency (inflection point) and n (Hill coefficient) determines the slope of the curve at the inflection point (Rospars et al. 1996). A spontaneous activity was attributed to each simulated neuron. Its rate F_0 was drawn from the distribution of the observed spontaneous firing rates. When $F(C)$ given by (1) was less than $1.25 \cdot F_0$, the ORN was considered as not responding and F was set to 0 at dose C and lower.

Latency $L(C)$ decreases to a horizontal asymptote L_m . It can be described by a decreasing exponential with 3 parameters λ , L_a and L_m (**Fig. 2b**):

$$L(C) = L_a \exp(-\lambda(C - C_a)) + L_m \quad (2)$$

where L_m is the asymptotic latency at high dose, $L_m + L_a$ is the latency at reference dose C_a (we took $C_a = -1 \log \text{ng}$ for all neurons) and λ determines the “slope” of the curve. When $L(C)$ given by (2) was more than 5 s, the ORN was considered as not responding at dose C and lower.

2.3. Stochastic model of a population of ORNs

The responses of the ORN population were summarized as a set of 6 statistical distributions, one distribution for each parameter of $F(C)$ and $L(C)$ functions. The distributions of F_M , $C_{1/2}$, $\ln n$, $\ln \lambda$, $\ln L_a$ and $\ln L_m$ were shown to be Gaussian. Each distribution was characterized by its mean μ_i and standard deviation σ_i . This is illustrated for F_M and L_m in **Fig. 3**.

However, these distributions were not independent. For example the dose at half-maximum frequency and the Hill coefficient n were significantly correlated (for a complete study of parameter distributions and correlations, see Grémiaux et al., in preparation). Standard deviations σ_i and correlations r_{ij} between pairs of parameters i and j were gathered into the symmetric variance-covariance matrix Σ . For example, if there were only three random variables, F_M ($i = 1$), $C_{1/2}$ ($i = 2$) and $\ln n$ ($i = 3$), Σ would be

$$\Sigma = \begin{pmatrix} \sigma_1^2 & r_{12}\sigma_1\sigma_2 & r_{13}\sigma_1\sigma_3 \\ r_{21}\sigma_2\sigma_1 & \sigma_2^2 & r_{23}\sigma_2\sigma_3 \\ r_{31}\sigma_3\sigma_1 & r_{32}\sigma_3\sigma_2 & \sigma_3^2 \end{pmatrix} \quad (3)$$

The tri-normal distribution that gives the probability to have a certain triplet of parameters (and therefore a certain dose-frequency curve) is completely given by its mean (μ_1, μ_2, μ_3) and its matrix Σ . All parameter triplets with a probability higher than any predefined value are located within an ellipsoid centred on point (μ_1, μ_2, μ_3) in the parameter space (**Fig. 4**).

Generalization to 6 parameters is straightforward. It involves the 6-dimensional multinormal distribution of mean M and variance-covariance matrix Σ , where M is a 6-element vector including the means of parameters F_M , $C_{1/2}$, $\ln n$, $\ln \lambda$, $\ln L_a$ and $\ln L_m$, and Σ is a 6-by-6 matrix in which all terms are of the form $r_{ij}\sigma_i\sigma_j$ as in (3). Each set of 6 values drawn at a time from the multinormal (M, Σ) distribution defines simultaneously the Hill $F(C)$ and exponential $L(C)$ response functions of a given ORN. The drawn values located outside the interquartile range including 95% of possible sets were discarded (**Fig. 4**).

2.4. Statistics

Normal and lognormal distributions were used. Both depend on two parameters, mean μ and standard deviation σ . The lognormal distribution is related to the normal distribution: if X is log-normally distributed, with parameters μ and σ , $\ln X$ follows a normal distribution of mean μ and standard deviation σ . Comparisons between distributions were tested using the Kolmogorov-Smirnov test at level 1%. All algorithms were written in Matlab and statistical analyses were done with the Matlab Statistics Toolbox (The MathWorks, Natick, USA).

2.5. Estimates of model parameters

From experimental recordings of ORNs stimulated with the main pheromone component (see section 2.1) we determined the frequencies F and latencies L at various doses C . The data points of the corresponding plots were fitted with three-parameter Hill (eq. 1) and exponential (eq. 2) functions respectively. Thus, each fitted ORN was fully characterized by a set of 6 parameters: its maximum firing rate (F_M), its apparent affinity for the pheromone ($C_{1/2}$), the “slope” (Hill coefficient n) of the $F(C)$ curve, its maximum (L_a) and minimum (L_m) latencies, and the “slope” (λ) of the $L(C)$ curve. All these parameters were well fitted to lognormal distributions, except F_M and $C_{1/2}$ which were Gaussian (Grémiaux et al., in preparation; see examples in **Fig. 3**). So each distribution could be completely described by only two parameters, mean μ_i and standard deviation σ_i . The 15 coefficients of correlation r_{ij} between the parameters were also taken into account. The resulting vector M of 6 elements (μ_i) and a variance-covariance matrix Σ of 21 different elements (σ_i and r_{ij}) are given in Table 1. These 27 numbers give a complete statistical description of the responses (F , L) yielded by any ORN at any dose. Interestingly, all r_{ij} between the groups of F and L parameters were shown to be nonsignificant (Grémiaux et al., in preparation), indicating that the rate and the latency parameters are independent as they are jointly normally distributed.

3. RESULTS

3.1. Validation of the stochastic model

For simulating the ORN population, the 6 parameters defining each ORN were drawn $N = 20\,000$ times from the multinormal distribution (M , Σ) defined in Table 1 (**Fig. 4**). The N dose-response curves obtained (**Fig. 5**) were examined at the six doses studied experimentally. For example, the N frequencies $F(1)$ at dose $C = 1$ were determined (see **Fig. 5a**) and their cumulated distribution was plotted (**Fig. 6c**). The distribution of latencies $L(1)$ (**Fig. 5b**) was also plotted (**Fig. 7c**). The same procedure was applied at the five other doses. The simulated distributions obtained with the multinormal (M , Σ') (dotted lines), where Σ' is the matrix with all nonsignificant correlations put to zero (Table 1), were practically identical to those obtained with Σ (solid lines).

These simulated distributions at six doses were then compared to the distributions of F and L determined from experimental recordings (**Figs. 6** and **7**). To take into account the uncertainty on the dose C delivered to the sensillum, we determined also the distributions of F and L at doses $C \pm 2.5\sigma_C$ (with $\sigma_C = 0.2C$) including 99% of C values. The simulated distributions are included in the 95% confidence interval of the experimental distributions and Kolmogorov-Smirnov tests confirmed that the simulated and observed distributions do not significantly differ, except for the upper limit of the confidence interval at dose $-1.5 \log \text{ ng}$ for F (**Fig. 6c**). Overall, the predicted firing frequencies and latencies are in agreement with their experimental counterparts.

3.2. Main features of the model

Next, we utilized the stochastic model to analyse the properties of the overall response of the whole population of pheromone-sensitive ORNs. The results obtained can be summarized as follows:

First, the modelled firing frequencies (**Figs. 6, 8a**) and the logarithms of the modelled latencies (**Figs. 7, 8b**) can be well approximated with normal (or truncated normal) distributions. Thus, the distributions of modelled F and L at various doses can be described by the means (μ_F , μ_L), standard deviations (σ_F , σ_L) and amplitudes (A_F , A_L) of their fitted (truncated) normal distributions (**Fig. 8a, b**).

Second, the distributions of F are narrow and low at low doses and tend to become wider and higher at high doses (**Fig. 8a**). The reverse is found for $\ln L$ (**Fig. 8b**). These effects show that the means μ_F and μ_L , standard deviations σ_F and σ_L , and amplitudes A_F and A_L of both distributions depend on the dose. Function $\mu_F(C)$ follows very closely a Hill function (**Figs. 8c, 9a**) and $\sigma_F(C)$ grows also according to a sigmoid curve (**Fig. 8e**). Function $\mu_L(C)$ (**Fig. 8d**) decreases exponentially (**Fig. 9b**), and $\sigma_L(C)$ (**Fig. 8f**) also quickly decreases on the same dose range. The amplitude function $A_F(C)$, which reflects the proportion of ORNs close to the mean population frequency decreases then stays approximately constant above $C = 1 \log ng$ (**Fig. 8g**), whereas the amplitude of the $\ln L$ distribution is practically zero below $C = -1 \log ng$ and then increases above according to a sigmoid curve (**Fig. 8h**). At all doses, the modelled properties (μ , σ , A) are in good agreement with the corresponding properties determined from the normal distributions fitted to the experimental distributions of F and L (crosses in **Fig. 8c-h**).

Third, the variability of responses across ORNs in the population can also be quantified by selecting the 5% most extreme responses at each dose, i.e. the lowest and highest frequencies and the shortest and longest latencies. Their plotted means show that the range between the extremes increases with the dose for frequencies (**Fig. 9a**), whereas it decreases for latencies (**Fig. 9b**) in accordance with the conclusions above based on standard deviations. However, although responses with high rates have short latencies (**Fig. 9c**), it is noteworthy that the ORNs with the highest frequencies are rarely those with the shortest latencies (**Fig. 9d**). This is confirmed by plotting the modelled latencies of the 5% ORNs with highest frequencies at various doses (one example is shown at $C = 0 \log ng$ in **Fig. 9e**); and similarly, the frequencies of the 5% ORNs with shortest latencies (**Fig. 9f**). These plots indicate that F and L are uncorrelated in the same ORNs. So, according to the model, a fast responding neuron can have a low firing rate and vice versa.

4. DISCUSSION

The model presented here focuses on ORNs in the moth antenna that respond to the main pheromone component. It summarizes in a few rules the essence of extracellular electrophysiological measurements performed on these neurons and generalizes them to describe the whole neural population. In short, the most significant part of the information contained in the original experimental data were summarized as (i) the dose-response functions, Hill functions for the peak frequency $F(C)$ and exponential functions for the latency of the first spike $L(C)$, (ii) the Gaussian nature of the statistical distributions of the six response parameters (or their logarithm) that appear in functions $F(C)$ and $L(C)$, and (iii) the mean vector M and variance-covariance matrix Σ that characterize the Gaussian distributions and their correlations. Although perfectible, this model appears reliable and of more general applicability.

4.1. Properties of the model

As shown in **Figs. 6** and **7** the distributions of firing rates and latencies predicted by our model at several doses are in broad agreement with those observed experimentally at the same doses. This result validates the suggestion that the multinormal distribution and the numerical values of its two parameters (means and variance-covariance matrix as given in Table 1) reflect in a compact form the main features of the ORN population studied.

The main properties of the population of pheromone-responsive ORNs are summarized in **Figs. 8** and **9**. A first significant feature is that the mean firing rate of the ORN population is a Hill function of the dose like in the individual ORNs (**Figs. 8c** and **9a**). This is also the case for the extreme responses (**Fig. 9a**). This result is not trivial because it is not true in general for the summation of any set of Hill functions. Therefore, it arises from the specific probability distributions in the population of the parameters describing individual ORNs and from the assumption that the neurons do not interact (see however Vermeulen and Rospars, 2004). The mere conservation of the single cell laws at the neural population level is a noteworthy simplifying property of this system. However, the situation is not as clear for latencies below the lowest tested dose ($-1 \log \text{ ng}$; **Fig. 9b**). Further experimental work is needed to decide whether the exponential function (eq. 2) provides a fully correct description of individual dose-latency curves at very low doses.

Another interesting feature concerns the distributions of firing frequencies at various doses as described by their mean, standard deviation and amplitude (**Fig. 8**, left column). These three functions of C are very similar to those found previously by Sandström et al. (2009; see their Figs. 4 and 5). This other model was also about an ORN population in which all neurons express the same olfactory receptor but it was built differently and its numerical values come from another system. Each ORN was described by a biophysical model taking into account its biochemical, electrical and geometrical characteristics (Rospars et al., 1996, 2003, 2008). The series of conversions taking place during transduction (activated receptors, ionic conductances, receptor potential and firing frequency) were summarized as four main equations with 13 parameters. The values of these parameters and their variability (normal or lognormal) were determined from experimental measurements of frog ORNs (Rospars et al., 2003). A population of ORNs was simulated with 9 of these parameters varying according to the normal (or lognormal) distributions found. This model predicts that at each dose the distribution of response frequencies across ORNs in the population is normal with mean μ_F , standard deviation σ_F and amplitude A_F . Moreover, it shows that $\mu_F(C)$ and $\sigma_F(C)$ both follow the same sigmoid function (that is not a Hill function, see eq. 8 in Sandström et al., 2009), and that the amplitude A_F is a quickly increasing then decreasing function of C (see their eq. 9).

The present work on moth ORNs confirms most of these predictions, with a few differences: in the moth ORN population $\mu_F(C)$ can be described by Hill functions and the amplitude A_F does not present the short initial rise to maximum, so that only the decreasing part is found. These differences likely result from the different effects of very low odorant doses in the frog and moth models due to the choice of different firing thresholds. Neglecting these second-order differences, the convergence of results from these independent models, built on widely different assumptions and whose parameters come from experiments on different types of ORNs (frog generalist and moth specialist ORNs) suggests that the basic qualitative and quantitative properties of the ORN populations remain the same whatever the ORN types and species considered. However, these common properties are likely not expressed on the same range of concentrations, the moth pheromone-sensitive ORNs having a lower threshold and a wider dynamic range than the frog generalist ORNs.

4.2. Perspectives

A better understanding of the peripheral olfactory code along the lines followed here should benefit from an extension of the experimental recordings and of their quantitative description, and from improvements of the model itself. Let's briefly discuss these three aspects.

Precise experiments on ORNs present difficulties at both ends of the dose axis. High doses ($>4 \log \text{ ng}$ depending on ORNs) must be avoided because they exhaust the neuron which may need several minutes to return to its resting state (several physiological processes can be saturated, like pheromone degradation, exchanger pumps for intracellular calcium etc.). At the low dose end, the model predicts the existence of ORN rare responses coming from neurons with very low thresholds and/or with very short latencies in the left tails of the corresponding distributions. Their small number explains that they are rarely found in the recorded samples (the ratio of sample size to number of pheromone-sensitive ORNs is only about 1%). However, they are essential to explain the responses of the projection neurons (PNs) to which the ORNs are connected in the MGC because the average PN has much lower threshold and shorter latency than the average ORN (Jarriault et al., 2009). These properties of PNs can be explained only if they selectively react to the ORNs with the lowest thresholds and shortest latencies (Grémiaux et al, in preparation). New experimental recordings closer to threshold and supplemented with adequate modelling will be indispensable to understand the properties of the system near its response threshold.

The description of the response in terms of firing rate and latency is sufficient for a first approach because these two variables reflect the most important properties of the spike trains. However, a complete description will require consideration of the evolution in time of the instantaneous firing rate in the course of the response. The response kinetics presents an initial peak (measured by F as defined in this work) followed by a fast adaptation and decrease to a lower rate. In vertebrates, the kinetics of the response is different with a silent period following the peak. This silence endows the population response with concentration-invariant properties (Rospars et al., in preparation) that are apparently not found in pheromone-sensitive ORNs.

The model does not rely on any assumption on the mechanisms behind the observed spike trains and involves only generalizations of the original data. It provides in a concise and easy-to-use form the essence of the extensive experimental observations made with the main component of the sex pheromone blend. It requires little computational resources and is therefore well suited to simulate the input of the ORN population to the MGC in the AL, which may be very useful for models of the MGC and AL, such as (Buckley and Nowotny, this issue). However, this phenomenological approach presents two limitations. First, because of the uncertainties discussed above, it is not known whether the Hill and exponential functions are exact descriptions of frequencies and latencies at both ends of the dose axis. This uncertainty is more acute for latencies below dose $-2 \log \text{ ng}$ where the exponential function predicts latencies too long to yield detectable responses (**Fig. 9b**). A function better suited to describe latency in this concentration range will have to be found. Second, the phenomenological nature of the model does not explain the variations observed across ORNs in the population. As noted above, several factors can explain this variability (Rospars et al., 2003; Sandström, 2009) including molecular (receptors, enzymes, ionic channels, pumps), geometrical (areas of various membrane parts) and electrical (membrane resistance etc.) factors that depend on one another (Gu and Rospars, 2011). The overall properties of the ORN population predicted by the present phenomenological model and the analytical model developed in Sandström et al. (2009) are consistent. This consistency indicates that the available biophysical models are detailed enough to relate the low-level neuron (and

sensillum) characteristics to their high-level (spike train) properties. This opens the way to an interpretation of the observed response variability of ORNs expressing the same olfactory receptor (Grosmaître et al., 2006; Jarriault et al., 2010) or different olfactory receptors (Rospars et al., 2003; 2008) that is essential for a proper understanding of cerebral olfactory processes.

ACKNOWLEDGMENTS

The authors are grateful to Dr David Jarriault and Dr Sylvia Anton for many discussions in the course of this work and to three anonymous referees for helpful suggestions. This work was funded by the Agence Nationale de la Recherche within the French-British ANR BBSRC SysBio 006 01 “Pherosys” initiative and the European FP7-ICT 2007 STREP Bio-ICT convergence “Neurochem”.

REFERENCES

- Bazhenov, M., Stopfer, M., Rabinovich, M., Huerta, R., Abarbanel, H.D.I., Sejnowski, T.J. Laurent, G, 2001. Model of transient oscillatory synchronization in the locust antennal lobe. *Neuron*, 30, 553-567.
- Chase, S.M., Young, E.D. (2007) First-spike latency information in single neurons increases when referenced to population onset. *Proc. Nat. Acad. Sci.*, 104, 5175-5180.
- Christensen, T.A., D'Alessandro, G., Lega, J., Hildebrand, J.G., 2001. Morphometric modeling of olfactory circuits in the insect antennal lobe: I. Simulations of spiking local interneurons. *BioSystems* 6, 143-153.
- Cleland, T.A., Linster, C., 2005. Computation in the olfactory system. *Chemical Senses* 30, 801-813.
- Cox, D. R., Oakes, D., 1984. *Analysis of Survival Data*, Chapman & Hall, London.
- Davis, R.L., 2004. Olfactory learning. *Neuron* 44, 31- 48.
- De Bruyne, M., Baker, T.C., 2008. Volatile codes: Odor detection in insects. *J. Chem. Ecol.* 34, 882-897.
- Grosmaître, X., Vassalli, A., Mombaerts, P., Shepherd, G., Ma, M., 2006. Odorant responses of olfactory sensory receptor neurons expressing the odorant receptor MOR23: a patch clamp analysis in gene-targeted mice. *Proc. Nat. Acad. Sci.*, 103, 1970-1975.
- Gu Y., Rospars J.-P., 2011. Dynamical modeling of the moth pheromone-sensitive olfactory receptor. *PLoS One* (in press).
- Hansson, B.S., Ljungberg H., Hallberg, E., Löfstedt, C., 1992. Functional specialization of olfactory glomeruli in a moth. *Science* 256: 1313-1315.
- Hildebrand, J.G., Shepherd G.M., 1997. Mechanisms of olfactory discrimination: converging evidence for common principles across phyla. *Annu. Rev. Neurosci.* 20, 595-631.
- Homberg, U., Montague R.A., Hildebrand J.G., 1988. Anatomy of antenno-cerebral pathways in the brain of the sphinx moth *Manduca sexta*. *Cell Tissue Res.* 254, 255-281.
- Ito, I., Bazhenov, M., Ong, R.C.Y., Raman B., Stopfer, M., 2009. Frequency transitions in odor-evoked neural oscillations. *Neuron*, 64, 692-706.
- Jacquin-Joly, E., Lucas, P., 2005. Pheromone reception and transduction: mammals and insects illustrate converging mechanisms across phyla. *Current Topics Neurochem.* 4, 75-105.
- Jarriault, D., Gadenne, C., Rospars, J.-P., Anton, S., 2009. Quantitative analysis of sex-pheromone coding in the antennal lobe of the moth *Agrotis ipsilon*: a tool to study network plasticity *J. Exp. Biol.* 212, 1191-1201.
- Jarriault, D., Gadenne, C., Lucas, P., Rospars, J.-P., Anton, S., 2010. Transformation of signal in the noctuid moth *Agrotis ipsilon*: from peripheral input to antennal lobe output. *Chemical Senses* 35, 705-715.
- Junek, S., Kludt, E., Wolf, F., Schild, D., 2010. Olfactory coding with patterns of response latencies. *Neuron* 67, 872-884.
- Kaissling, K-E., Rospars, J-P., 2004. Dose-response relationships in an olfactory flux detector model revisited. *Chem. Senses* 29, 529-531 & Erratum 529, 747.
- Kay, L.M., Stopfer, M., 2006. Information processing in the olfactory systems of insects and vertebrates. *Seminars Cell. Dev. Biol.* 17, 433-442.
- Krofczik, S., Menzel, R., Nawrot, M.P. (2009) Rapid odor processing in the honeybee antennal lobe network. *Frontiers Comput. Neurosci.*, 2: article 9, 1-13.
- Martinez, D, 2005. Oscillatory synchronization requires precise and balanced feedback inhibition in a model of the insect antennal lobe. *Neural Computation* 17, 2548-2570.

- Raman, B., Joseph, J., Tang, J., Stopfer, M., 2010. Temporally diverse firing patterns in olfactory receptor neurons underlie spatiotemporal neural codes for odors. *J. Neurosci.* 30, 1994-2006.
- Rospars, J.-P., 1988. Structure and development of the insect antennodeutocerebral system. *Int. J. Insect Morphol. Embryol.* 17, 243-294.
- Rospars, J.-P., Fort J.-C., 1994. Coding of odour quality: roles of convergence and inhibition. *Network: Computation in Neural Systems* 5, 121-145.
- Rospars, J.-P., Lansky, P., Tuckwell, H.C., Vermeulen, A., 1996. Coding of odor intensity in a steady-state deterministic model of an olfactory receptor neuron. *J. Comp. Neurosci.* 3, 51-72.
- Rospars, J.-P., Lansky, P., Duchamp-Viret, P., Duchamp, A., 2003. Relation between stimulus and response in frog olfactory receptor neurons in vivo. *Eur. J. Neurosci.* 18, 1135-1154.
- Rospars, J.-P., Lansky, P., Chaput, M., Duchamp-Viret, P., 2008. Competitive and noncompetitive odorant interactions in the early neural coding of odorant mixtures. *J. Neurosci.* 28, 2659-2666.
- Sandström, M., Lansner, A., Hellgren-Kotaleski, J., Rospars, J.-P., 2009. Modelling the response of population of olfactory receptor neurons to an odorant. *J. Comput. Neurosci* 27, 337-355.
- Simoes de Souza, F.M., Antunes, G., 2007. Biophysics of olfaction. *Rep. Prog. Phys.* 70, 451-491.
- Strausfeld, N.J., Hildebrand, J.G., 1999. Olfactory systems: common design, uncommon origins? *Curr. Opin. Neurobiol.* 9, 634-639.
- Vermeulen, A., Rospars, J.-P., 2004. Why are insect olfactory neurons grouped into sensilla? The teachings of a model investigating the effects of electrical interaction between neurons on the transepithelial potential and the neuronal transmembrane potential. *European Biophysics J.* 33, 633-643.
- Vosshall, L.B., Wong, A.M., Axel, R., 2000. An olfactory sensory map in the fly brain. *Cell* 102, 147-159.
- Zavada, A., Buckley, C.L., Martinez, D., Rospars, J.-P., Nowotny, T., 2011. Competition-based model of pheromone component ratio detection in the moth. *PLoS One*, 6 (2), e16308.

Table 1. Parameters of the multinormal distribution

Parameters		F_M	$C_{1/2}$	$\ln n$	$\ln L_a$	$\ln \lambda$	$\ln L_m$	
Mean	M	μ	219	0.87	-0.98	5.70	-0.04	3.72
Covariance	Σ^a	F_M	1958	9.37	-11.98	-24.18	-11.44	-13.64
		$C_{1/2}$	9.37	0.64	-0.11	-0.36	0.20	0.06
		$\ln n$	-11.98	-0.11	0.19	0.24	0.08	0.002
		$\ln L_a$	-24.18	0.36	0.24	1.88	0.56	0.07
		$\ln \lambda$	-11.44	0.20	0.08	0.56	0.45	0.26
Covariance	Σ'^b	F_M	1958	0	-11.98	0	0	0
		$C_{1/2}$	0	0.64	0	0	0	0
		$\ln n$	-11.98	0	0.19	0	0	0
		$\ln L_a$	0	0	0	1.88	0.56	0
		$\ln \lambda$	0	0	0	0.56	0.45	0.26
		$\ln L_m$	0	0	0	0	0.26	0.69

^a Original matrix Σ calculated with eq. (3); units as in Fig. 4

^b Simplified matrix Σ' with non-significant correlations ($p > 0.05$) put to zero

FIGURE LEGENDS

Figure 1. Example of responses of a moth pheromone-sensitive ORN. The major pheromone component (Z7-12:OAc) arrived at the antenna at time zero (vertical dashed line) and was applied for 200 ms (bar on the bottom line) with loads of 0.1, 1, 10, 100, 1000 and 10^4 ng on filter paper (corresponding to doses $C = -1, 0, 1, 2, 3$ and $4 \log \text{ ng}$, respectively). Spontaneous spikes are visible in the absence of pheromone before the stimulation.

Figure 2. Dose-frequency $F(C)$ and dose-latency $L(C)$ functions. (a) Hill function $F(C)$ given by eq. (1) showing maximum asymptotic response F_M , dose at half-maximum frequency $C_{1/2}$. (b) Decreasing exponential function $L(C)$ given by eq. (2) showing parameter L_a at dose C_a ($-1 \log \text{ ng}$ for all latency curves) and minimum asymptotic latency L_m . Parameter λ is related to the ‘slope’ of the curve. The parameter values of the curves shown are the means M given in Table 1.

Figure 3. Examples of cumulative histograms of the parameters of dose-frequency and dose-latency curves. (a) Distribution of maximum firing frequency F_M . Observed values (32, staircase graph) with fitted cumulative normal distributions (dotted) and corresponding probability density functions (dashed) providing mean and variance for F as given in Table 1. (b) Distribution of minimum latency L_m (18 values). Same representation as in (a).

Figure 4. Multinormal distributions of parameters defining dose-frequency and dose-latency functions. (a) Example of the binormal probability distribution function (pdf) of ($F_M, C_{1/2}$). (b) Trinormal pdf of the parameters ($F_M, C_{1/2}, \ln n$) of $F(C)$ in eq. (1) with projections of binormals on the three planes; as n follows a lognormal distribution, the logarithmic transform $\ln n$ was used. Based on $N = 20\,000$ drawings. (c) Trinormal pdf of the parameters ($\ln L_M, \ln \lambda, \ln L_m$) of $L(C)$ in eq. (2). Mean μ and standard deviation σ of normal distributions of parameters, without transformation ($F_M, C_{1/2}$) or after logarithmic transformation (all other parameters), are given in Table 1. The ellipsoids shown contain 95% of points. The darker the dots, the lower the probability to find the corresponding triplet. The F and L distributions are shown separately for illustration purposes only. In all other figures the six-dimensional multinormal distribution of parameters M and Σ given in Table 1 was used.

Figure 5. Examples of simulated (a) dose-frequency $F(C)$ and (b) dose-latency $L(C)$ curves. Ten vectors of six response parameters were drawn from the multinormal distribution defined in Table 1. The vertical dashed line at $C = 1 \log \text{ ng}$ shows some of the frequencies in (a) and latencies in (b) used to determine the statistical distributions shown in Figs. 6c and 7c. The latency and the corresponding frequency (same neuron, same dose) are represented with the same symbol and line style. Dose-response curves are truncated for latency $> 5 \text{ s}$ and/or frequency $< 1.2 F_0 \text{ AP/s}$ with spontaneous firing rate F_0 drawn from a lognormal distribution of parameters $\mu = 0.91$ and $\sigma = 0.91$.

Figure 6. Cumulated distributions of modelled firing frequencies at six doses ($-1, 0, 1, 2, 3$ and $4 \log \text{ ng}$) and comparison with experimental data. The non-responding neurons ($F = 0$) were taken into account in the statistics. Distributions of experimental frequencies ($N = 32$) shown as staircase graphs (solid line) with 95% confidence intervals (dashed lines) calculated using Greenwood’s formula (Cox and Oakes, 1984). Distributions of modelled frequencies shown as smooth curves based on $N = 20\,000$ drawings from the complete variance-covariance matrix Σ (solid line) or simplified matrix Σ' (dotted line) shown in Table 1. Simulations at $C \pm 0.5 \log \text{ ng}$ (see text) based on matrix Σ shown as dashed lines. All

modelled distributions are not significantly different from experimental distributions except for the upper limit of the confidence interval at dose $C = -1.5 \log \text{ ng}$ in (a) (Kolmogorov-Smirnov tests at level 1%).

Figure 7. Cumulated distributions of modelled response latencies at six doses and comparison with experimental data. Same representation as in Fig. 6 with $\ln L$ ($N = 18$). Modelled distributions are not significantly different from experimental distributions (Kolmogorov-Smirnov tests at level 1%).

Figure 8. Distributions of firing frequencies (left column) and latencies (right column) in the whole ORN population predicted by the model. (a) Distributions of modelled F at $C = -1, 1$ and $3 \log \text{ ng}$ can be approximated with normal or truncated normal distributions. The inset shows the three characteristics (μ, σ, A) used in (c-h). (b) Distributions of modelled $\ln L$ at the same doses as in (a) can be also approximated with normal or truncated normal distributions. (c, d) Mean μ , (e, f) standard deviation σ , and (g, h) amplitude A of the normal or truncated normal distributions fitted to the distributions shown in (a) and (b) as functions of C ; A gives the percentage of ORNs in the population with frequencies or latencies in the interval $\mu_F(C) - 20$ to $\mu_F(C) + 20$ AP/s and $\mu_L(C) - 25$ to $\mu_L(C) + 25$ ln ms. All plots are based on $N = 20\,000$ drawings from the multinormal distribution (M, Σ) given in Table 1. Plus symbols indicate the characteristics (μ, σ, A) of the normal or truncated normal distributions fitted to the experimental distributions.

Figure 9. Reconstructed summated response of the whole ORN population. (a) Mean frequency (solid) and its fitted Hill function (dot). Mean of the 5% highest and lowest rates (solid) and their fitted Hill functions (dot). (b) Same representation for latency. Mean latency fitted to the exponential (2) (dot). (c) Plot of pairs of firing rates and latencies at doses $-1, 0, 1, 2, 3$ and $4 \log \text{ ng}$ with $20\,000$ pairs per dose. The dashed curve shows how the mean firing rate (solid curve in panel a) depends on the mean latency (solid curve in panel b) at the same dose. (d) Plot of the 5% extreme firing rates and latencies at $C = 0$ (1000 pairs) showing the rarity of responses both strong and rapid. (e) Plot of the 1000 highest frequencies found at $C = 0 \log \text{ ng}$ and the latencies of the same responses; they are uncorrelated ($r = 0.032, p = 0.31$). (f) The 1000 shortest latencies at $C = 0 \log \text{ ng}$ and the frequencies of the same responses are also uncorrelated ($r = 0.028, p = 0.38$).

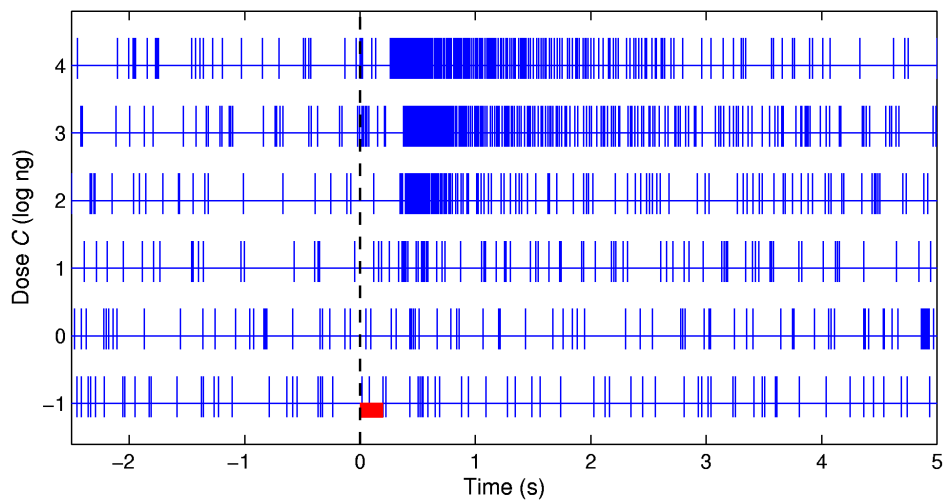


Fig. 1

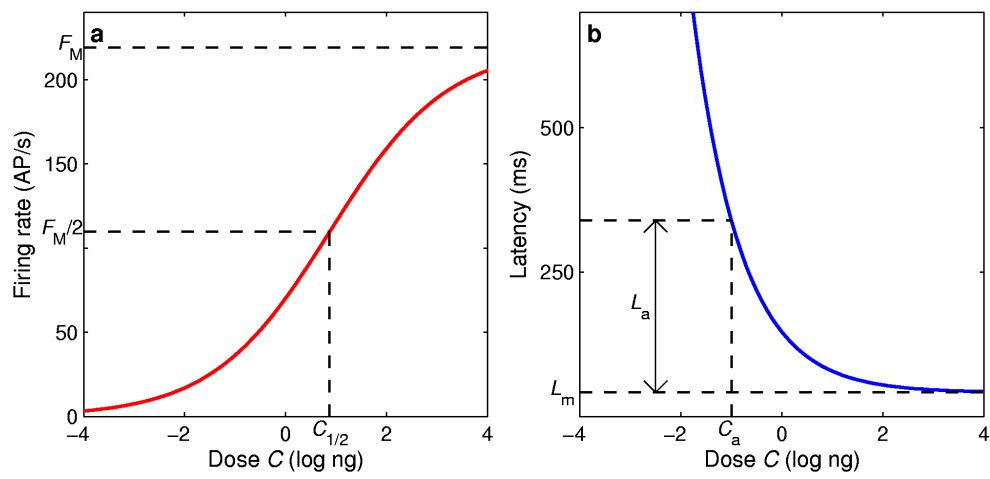


Fig. 2

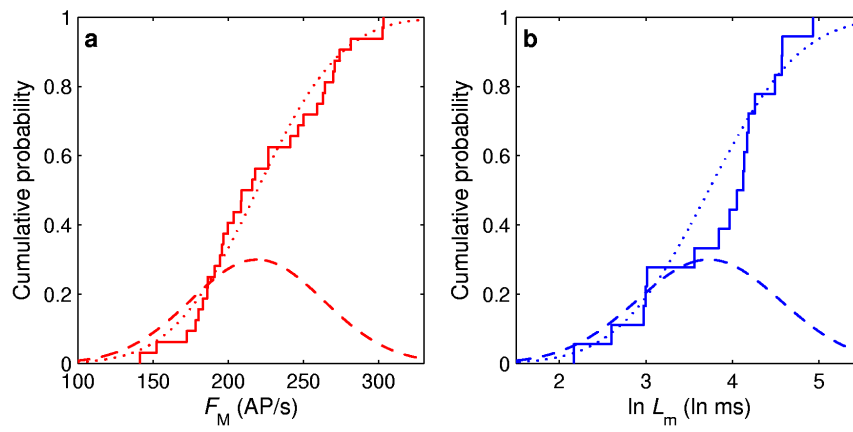


Fig. 3

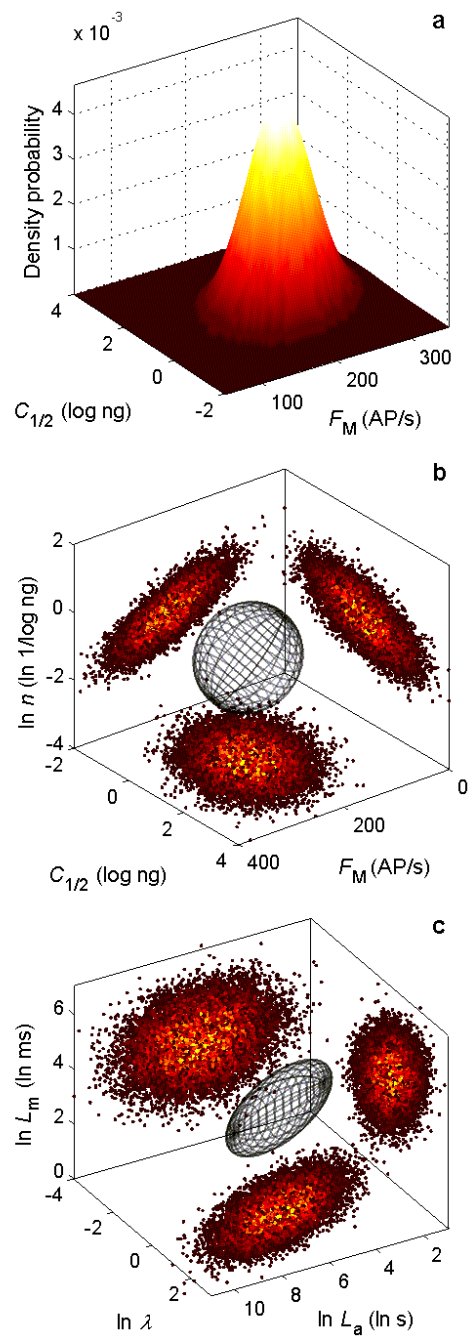


Fig. 4

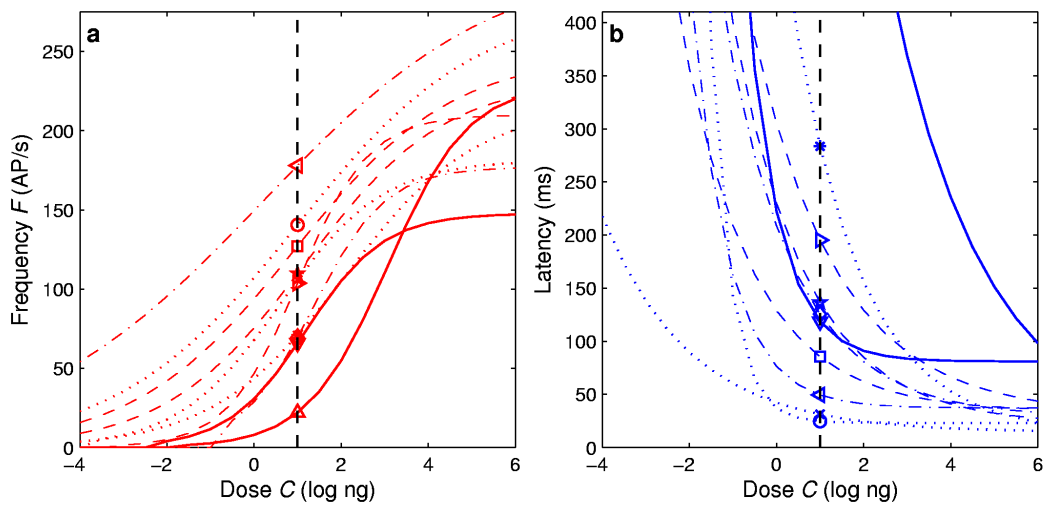


Fig. 5

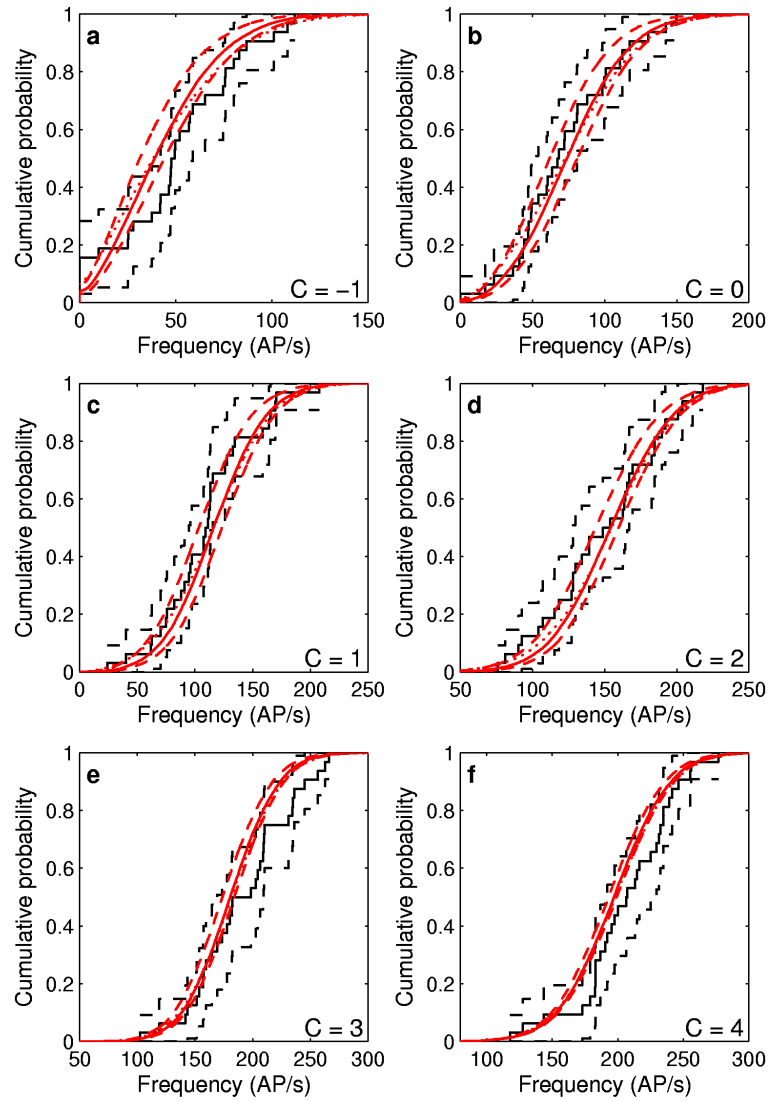


Fig. 6

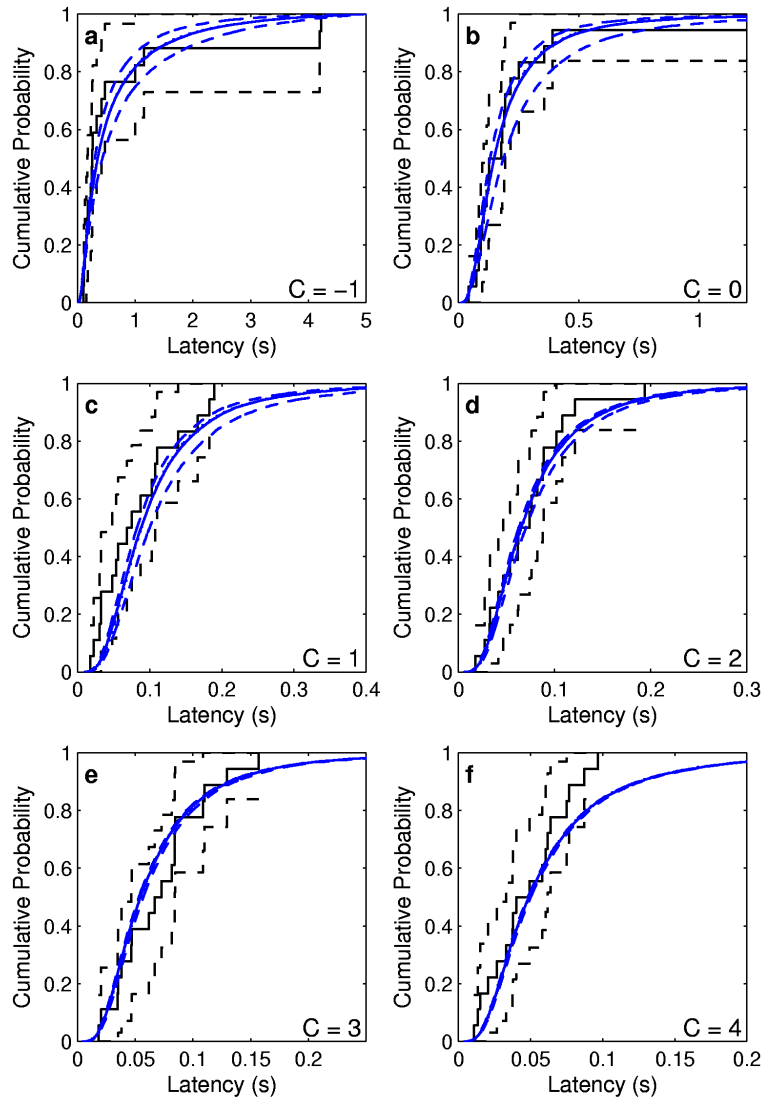


Fig. 7

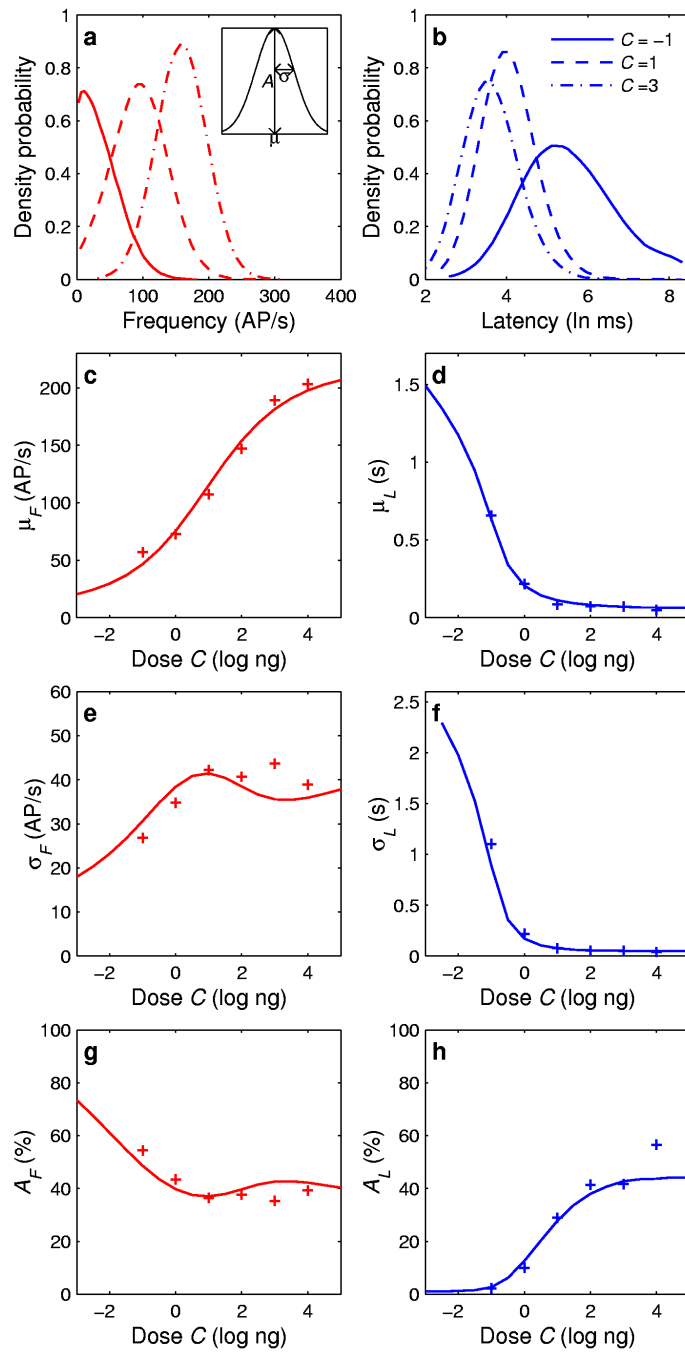


Fig. 8

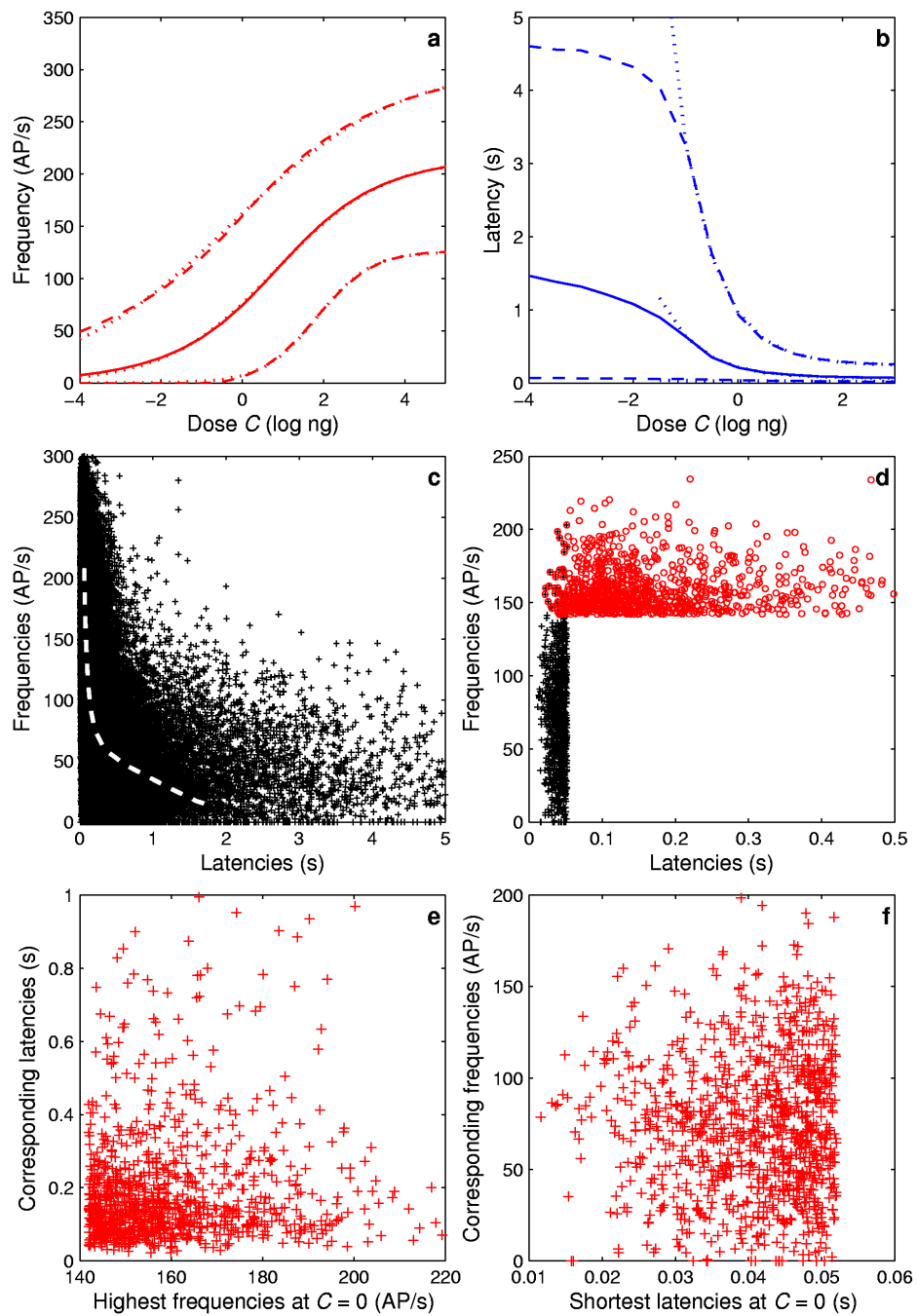


Fig. 9